

Supporting Information

Mechanistic Insights into the Rhodium- Catalyzed Aryl C–H Carboxylation

Liu, et al

Table of Contents

1. The full optimized structure of rhodium catalysts.....	S03
2. The thermodynamic data of pre-activation	S03
3. The coordination state of initially rhodium dimer.....	S03
4. The strategies for rhodium dimer dissociation	S04
5. The ligand exchange between hemicarbonatate and acetate	S04
6. The other possible C-H bond activation methods.....	S05
7. The acetate dissociation on earlier intermediates	S05
8. The spontaneous rearrangement of Rh8.....	S06
9. The scan data of direct carboxylation in the Rh-O site	S07
10. the direct carboxylation pathway from Rh7	S07
11. The other schemes of lactonization from Rh14 or Rh14'.....	S07
12. Proton transfer and lactonization after Rh-O carboxylation	S09
13. Comparison of the ability of different proton receptors	S09
14. The scheme of CO ₂ directly insert into the Rh-C bond of Rh4	S10
15. Gibbs free energy data of different bases (and conjugated acids).....	S10
16. More O'Ferrall-Jencks Plots	S11
17. The influence of phosphine ligands on reactivity.....	S12
18. Reference	S13

1. The full optimized structure of rhodium catalysts

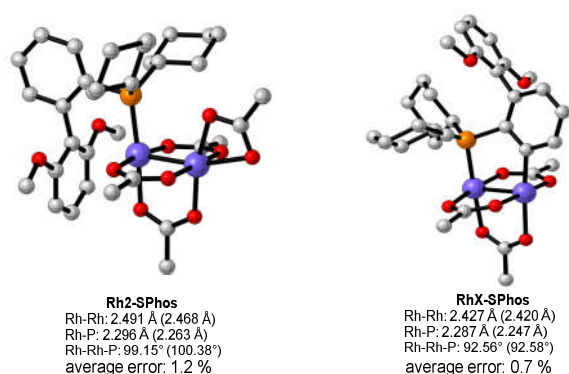


Figure S1. The full optimized structure of rhodium catalysts, the X-ray single-crystal diffraction data¹ is shown in brackets.

2. The thermodynamic data of pre-activation

The excessive ^tBuOK could react with **1a** to afford the potassium phenate (**1aK**) with a free energy decrease of 21.7 kcal/mol (Figure S2). CO₂ can react with the generated **1aK**, ^tBuOH and the remaining ^tBuOK (eq. 1-3), and the results indicate that the remaining ^tBuOK would transform to ^tBuOCO₂K.

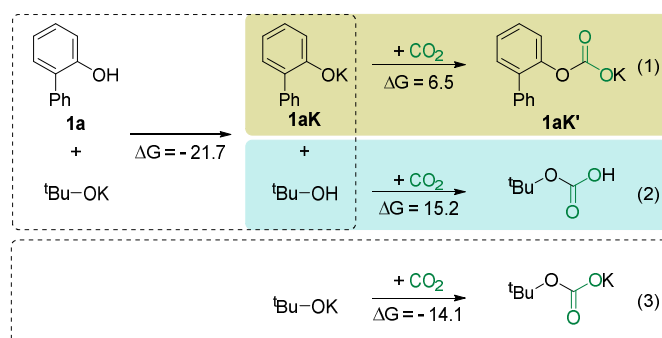


Figure S2. Thermodynamic data of acid-base reaction in the system

3. The coordination state of initially rhodium dimer

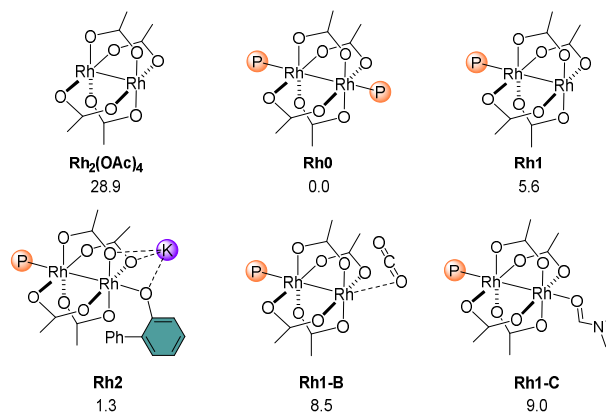


Figure S3. Gibbs free energy of rhodium dimer in different states (ΔG are given in kcal/mol, P = PCy₃).

4. The strategies for rhodium dimer dissociation

Combining the calculation results (Figure S4) and X-ray diffraction data of Li et al.,¹ the dissociation of the rhodium dimer catalyst was hard to achieve under the current reaction conditions.

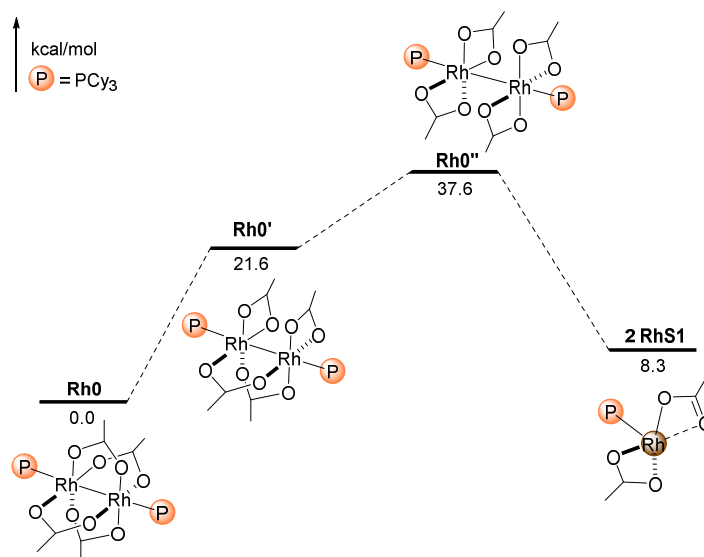


Figure S4. Gibbs free energy profiles of the rhodium catalyst dissociation

5. The ligand exchange between hemicarboxylate and acetate

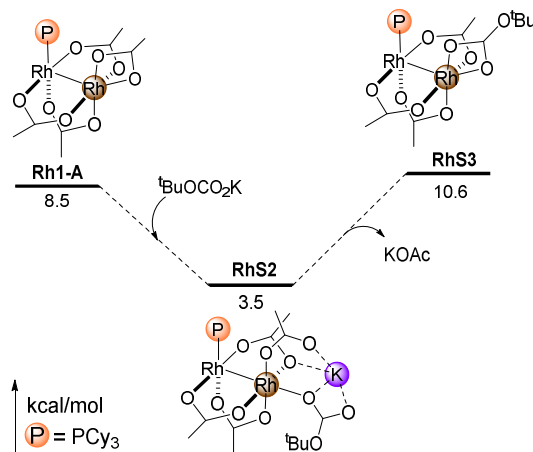


Figure S5. Gibbs free energy profiles of ligand exchange between hemicarboxylate and acetate

6. The other possible C-H bond activation methods

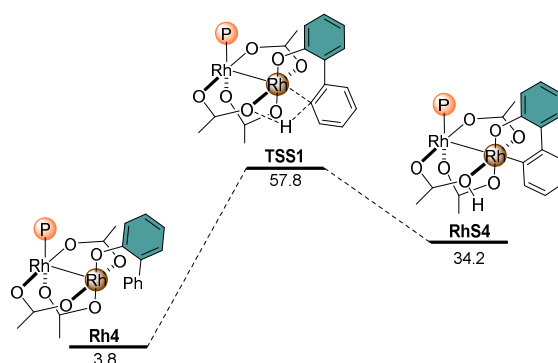


Figure S6. Gibbs free energy profiles of the C-H bond cleavage step via 1,2-addition.

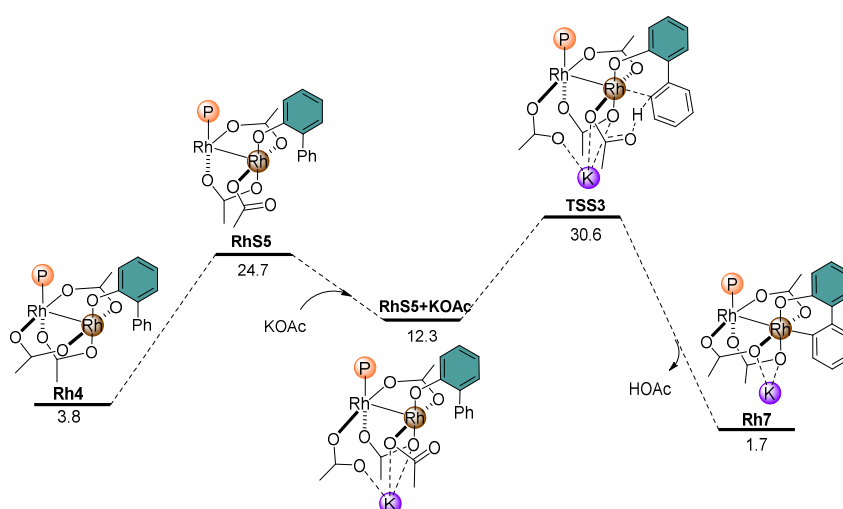


Figure S7. Gibbs free energy profiles of the C-H bond cleavage step via internal base Ac⁻.

7. The acetate dissociation on earlier intermediates

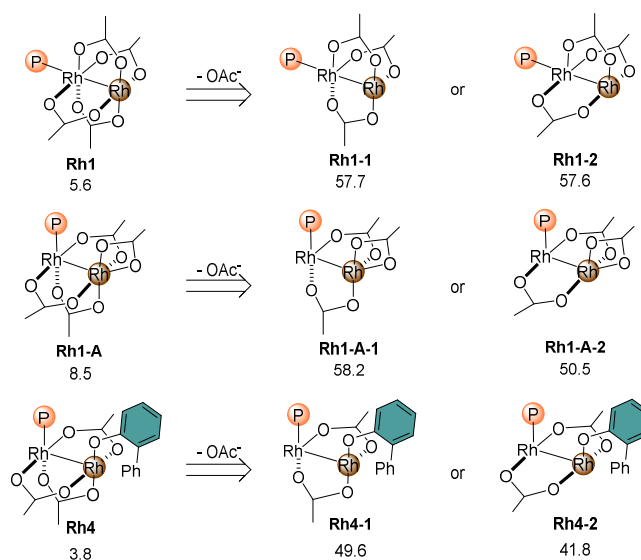


Figure S8. Acetate dissociation on the earlier intermediates (ΔG are given in kcal/mol, P = PCy₃)

8. The spontaneous rearrangement of Rh8

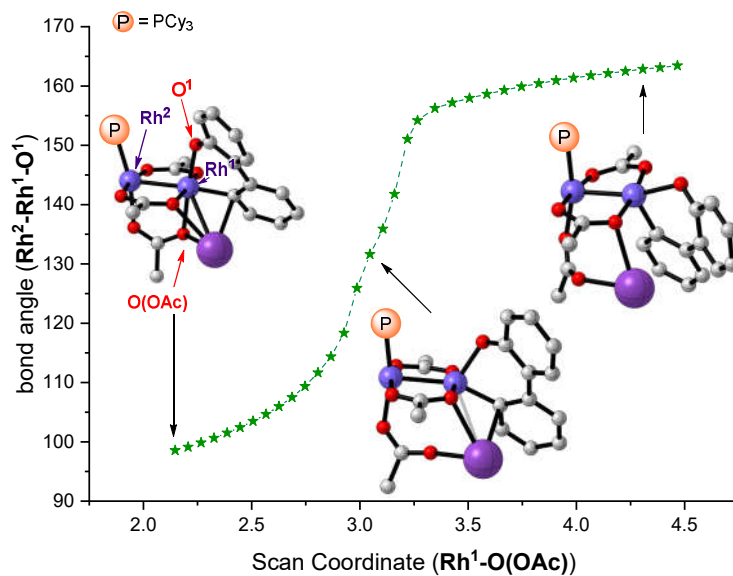


Figure S9. The scan data of **Rh7** dissociated potassium acetate to produce **Rh8**.

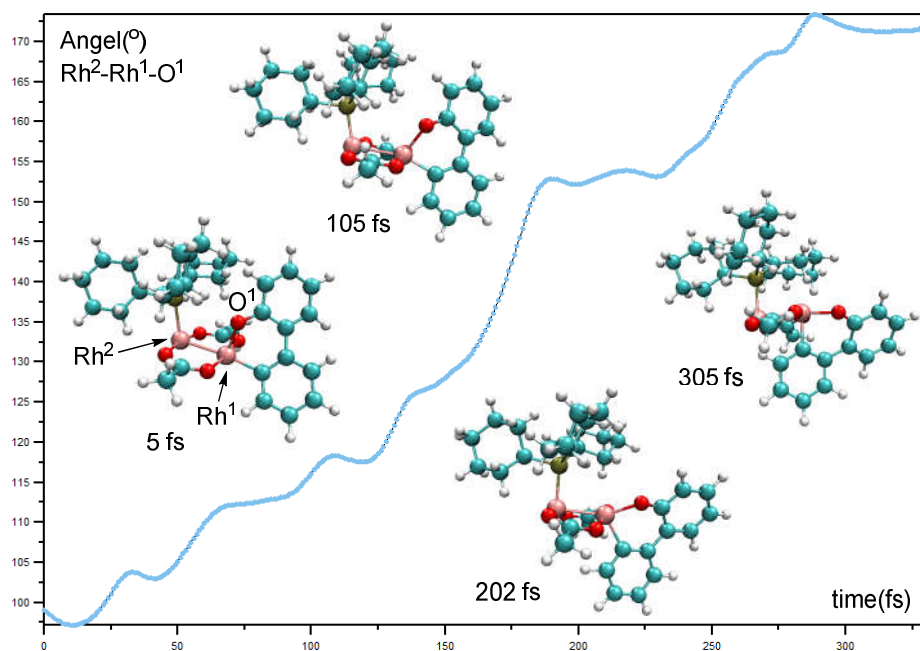


Figure S10. The bond angle ($\text{Rh}^2\text{-Rh}^1\text{-O}^1$) relationship of **Rh8** in molecular dynamics analysis via ORCA 5.0.1 program² and VMD 1.9.3³ (Functional: B97-3c,⁴ $T = 373.15$ K, timestep = 1.0 fs).

9. The scan data of direct carboxylation in the Rh-O site

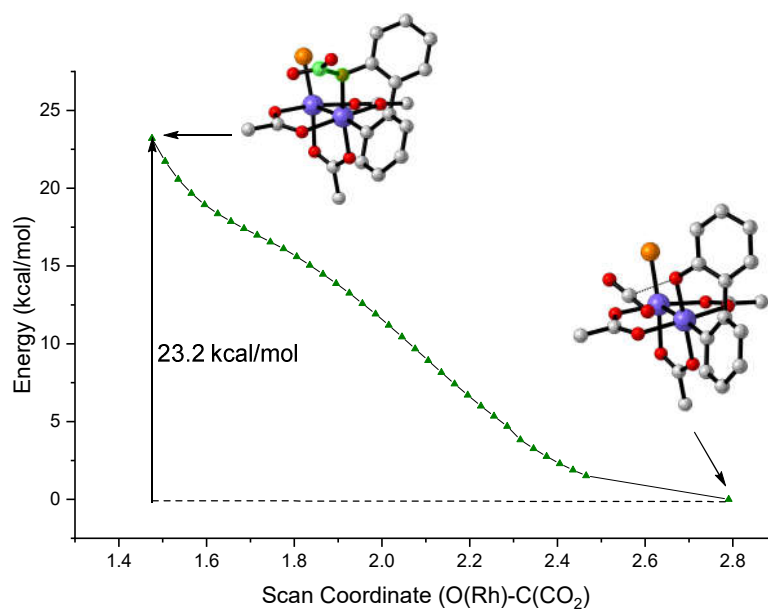


Figure S11. The scan data of direct carboxylation in the Rh-O site from Rh15 to Scan-TS4.

10. the direct carboxylation pathway from Rh7

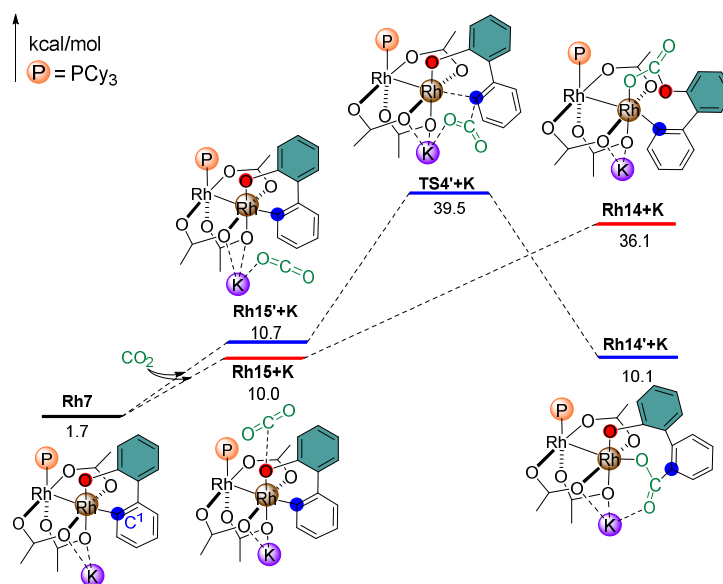


Figure S12. Gibbs free energy profiles of the direct carboxylation pathway from Rh7.

11. The other schemes of lactonization from Rh14 or Rh14'

(i) The direct lactonization pathways

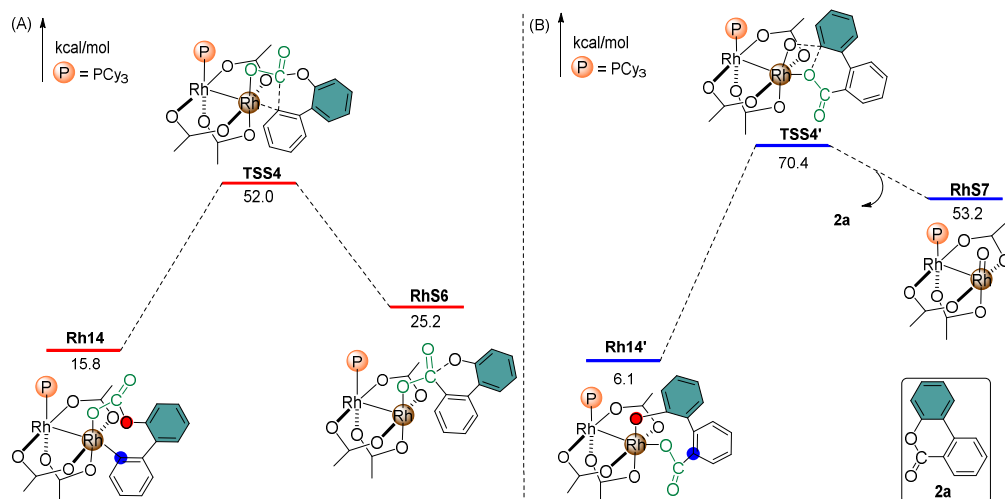


Figure S13. Gibbs free energy profiles of the direct lactonization from **Rh14** (A) or **Rh14'** (B) species.

(ii) The CO₂-assisted lactonization pathways

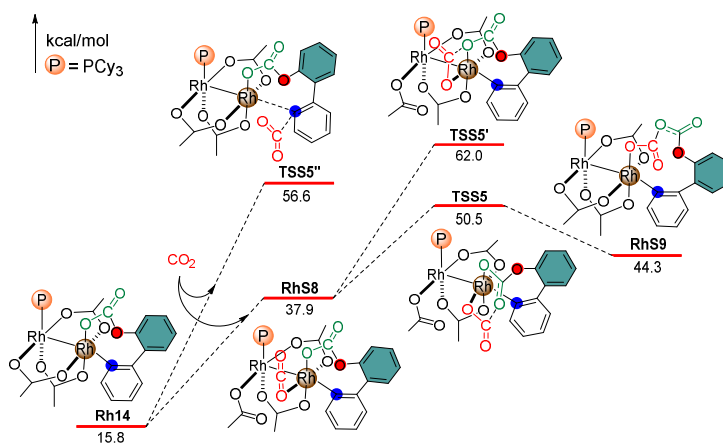


Figure S14. Gibbs free energy profiles of the CO₂-assisted lactonization from **Rh14**.

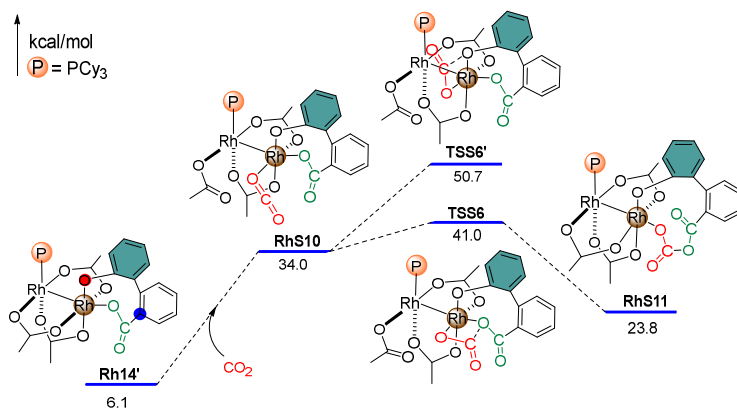


Figure S15. Gibbs free energy profiles of the CO₂-assisted lactonization from **Rh14'**.

(iii) The CO₂-assisted rearrangement and lactonization pathways

After the O¹ atom of **Rh14'** dissociated and rearranged to four-membered metallacycle species

RhS13, then go through the CO₂ insertion to form **RhS14**. In addition, the O¹ atom of **Rh12** could also be electrophilically attacked by CO₂ to generate a ten-membered metallacycle species **RhS16**. And then transfer into the six-membered metallacycle species **RhS17**. Unfortunately, the energy barriers of these two options are both beyond the allowable value.

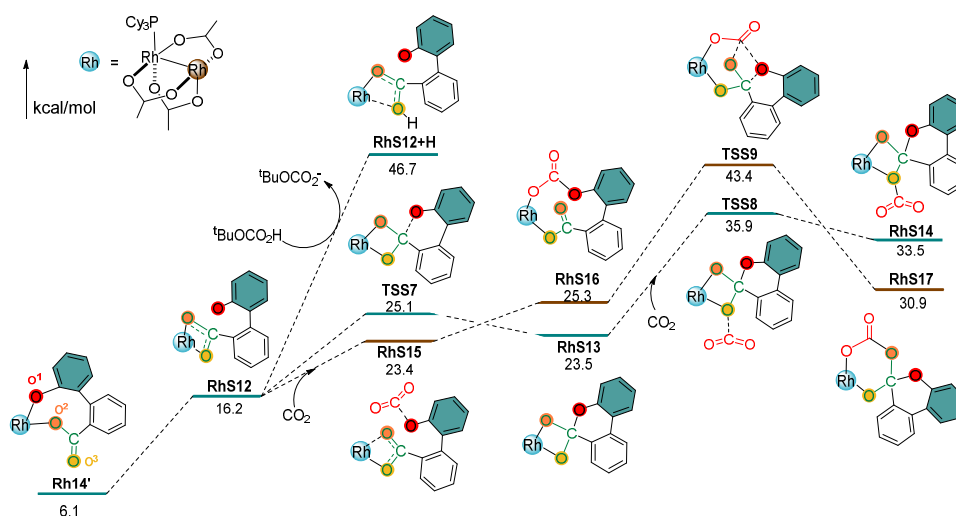


Figure S16. Gibbs free energy profiles of the lactonization with **Rh14'**.

12. Proton transfer and lactonization after Rh-O carboxylation

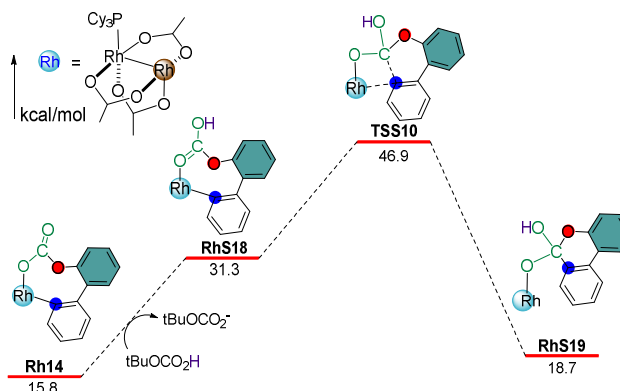


Figure S17. Gibbs free energy profiles of the lactonization steps after protonation of **Rh14**.

13. Comparison of the ability of different proton receptors

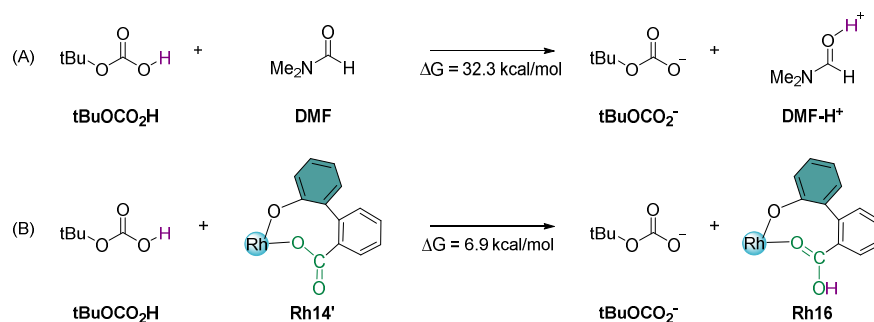


Figure S18. Comparison of the ability of different proton receptors to capture protons.

14. The scheme of CO₂ directly insert into the Rh-C bond of Rh4

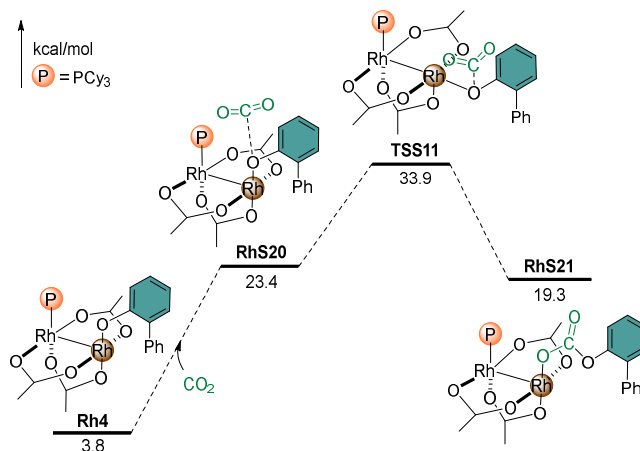


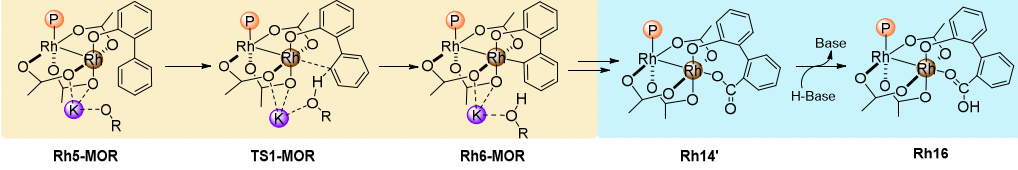
Figure S19. Gibbs free energy data of CO₂ insertion with Rh4.

15. Gibbs free energy data of different bases (and conjugated acids)

^tBuOK and the corresponding derivatives have been performed to produce potassium phenate (in the form of ^tBuOK), facilitate the C-H metalation (in the form of ^tBuOCO₂K), and mediate the lactonization (in the form of ^tBuOCO₂H).

From the calculated data in Table S1, it can be found that AcOK, ^tBuOCO₂K, MeOCO₂K and KHCO₃ can simultaneously satisfy the C-H bond activation and protonation. However, AcOK and KHCO₃ are not acidic enough to convert phenol to potassium phenate. ^tBuOCO₂K and MeOCO₂K can be obtained from the corresponding potassium alkoxide. Therefore, potassium alkoxide is an effective additive for reaction. Carbonate may also be suitable,¹ because carbonate and phenol can react to obtain bicarbonate, which then participates in the subsequent process.

Table S1. Gibbs free energy data of C-H bond activation with bases



Base (KOR)	Rh5-MOR	TS1-MOR	Rh6-MOR	ΔG^{\ddagger} (C-H activation)	ΔG^{\ddagger}	H-Base	ΔG^{\ddagger} (Proton Transfer)	pKa
KOH	2.7	9.5	-24.4	-27.1	6.8	H ₂ O	45.1	41.3
tBuOK	2.6	11.1	-22.6	-25.2	8.5	tBuOH	39.4	39.2
MeOK	4.0	11.5	-18.9	-21.0	9.4	MeOH	37.9	37.9
K ₂ CO ₃	4.3	14.6	-17.3	-21.5	10.3	KHCO ₃	34.8	35.1
AcOK	5.9	25.0	7.6	3.2	19.1	AcOH	12.8	21.9
tBuOCO ₂ K	4.0	23.8	5.1	1.1	19.8	tBuOCO ₂ H	7.0	18.3
MeOCO ₂ K	4.4	26.4	9.4	5.0	22.0	MeOCO ₂ H	6.2	17.9
KHCO ₃	6.4	28.2	12.8	6.9	21.8	H ₂ CO ₃	4.9	17.2
CF ₃ CO ₂ K	6.5	36.8	24.3	17.8	30.3	CF ₃ CO ₂ H	-8.3	9.2
KOPiv	4.2	22.3	6.8	2.6	18.1	HOPIv	11.8	21.3
AllylCO ₂ K	3.7	24.9	5.9	2.2	21.2	AllylCO ₂ H	11.9	21.3
CH ₂ FCO ₂ K	4.5	27.4	14.6	10.1	22.9	CH ₂ FCO ₂ H	5.8	17.7
EtCO ₂ K	4.8	24.0	5.6	0.8	19.2	EtCO ₂ H	10.3	20.4
nPrCO ₂ K	4.2	22.9	4.9	0.8	18.7	nPrCO ₂ H	14.6	23.0
BnCO ₂ K	5.7	23.6	6.3	0.5	17.9	BnCO ₂ H	12.9	21.9
PhCO ₂ K	3.6	24.6	9.9	6.3	20.9	PhCO ₂ H	9.7	20.0

16. More O’Ferrall-Jencks Plots

More O’Ferrall-Jencks plots⁵ were constructed using Wiberg bond orders of M-C and C-H bonds. These bond orders were calculated using the Natural Bond Orbital (NBO)⁶ software. In the More O’Ferrall-Jencks plots, the lines separating the CMD and the BIES regime were consequently constructed by connecting intermediate **Rh5** (the starting point of the C-H metalation process) with intermediate **Rh6**, which represents the C-H metalation product.

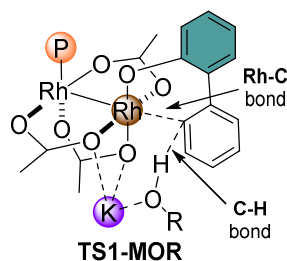


Table S2. Wiberg bond orders of M-C and C-H bonds.

Wiberg bond orders	Rh5-MOR		TS1-MOR		Rh6-MOR	
	C-H bond	Rh-C bond	C-H bond	Rh-C bond	C-H bond	Rh-C bond
^t BuOK	0.893	0.0708	0.525	0.324	0.001	0.722
KHCO ₃	0.893	0.0688	0.321	0.465	0.008	0.717
K ₂ CO ₃	0.884	0.1056	0.457	0.379	0.002	0.712
^t BuOCO ₂ K	0.893	0.0686	0.348	0.443	0.001	0.722
KOAc	0.893	0.0686	0.358	0.441	0.001	0.724

17. The influence of phosphine ligands on reactivity

As suggested by Houk et al.,⁷ the structure of the transition state is artificially divided into two parts, one is the CO₂-part, and the rest is labeled Rh-Part. Interestingly, the interaction energy (ΔE_{int}) negatively correlates with the carboxylation elementary step (ΔG^\ddagger). In contrast, there exists a positive correlation between the distortion energy ($\Delta E_{dist} = \Delta E_{dist-Rh} + \Delta E_{dist-CO_2}$) and ΔG^\ddagger .

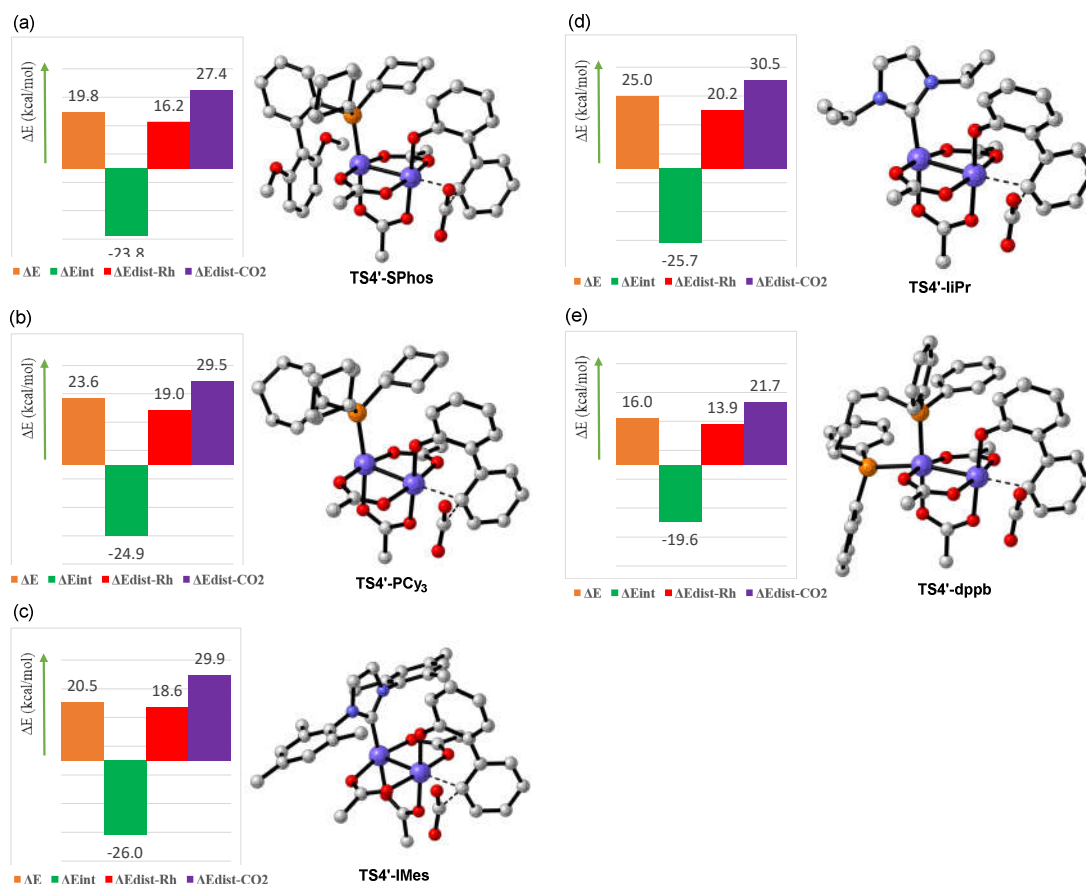


Figure S20. The distortion/interaction model analysis of **TS4'** with different ligands. (all the electron energies are obtained at the level of M06-D3/6-311+G(d,p)//SDD)

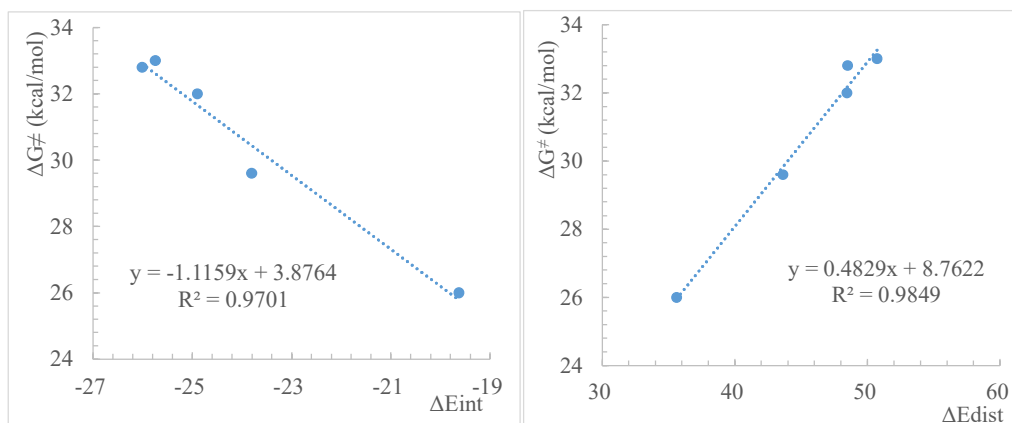


Figure S21. The relationship between energy barrier and interaction energy or distortion energy.

18. Reference

- (1) Fu, L.; Li, S.; Cai, Z.; Ding, Y.; Guo, X.-Q.; Zhou, L.-P.; Yuan, D.; Sun, Q.-F.; Li, G. Ligand-Enabled Site-Selectivity in a Versatile Rhodium(II)- α -Catalyzed Aryl C–H Carboxylation with CO_2 . *Nat. Catal.* **2018**, *1*, 469-478.
- (2) (a) Neese, F. Software Update: The ORCA Program System, Version 4.0. *WIREs Comput. Mol. Sci.* **2018**, *8*, e1327. (b) Neese, F. The ORCA Program System. *WIREs Comput. Mol. Sci.* **2012**, *2*, 73-78.
- (3) Humphrey, W.; Dalke, A.; Schulten, K. Vmd: Visual Molecular Dynamics. *J. Mol. Graphics* **1996**, *14*, 33-38.
- (4) Brandenburg, J. G.; Bannwarth, C.; Hansen, A.; Grimme, S. B97-3c: A Revised Low-Cost Variant of the B97-D Density Functional Method. *J. Chem. Phys.* **2018**, *148*, 064104.
- (5) (a) Jencks, W. P. General Acid-Base Catalysis of Complex Reactions in Water. *Chem. Rev.* **1972**, *72*, 705-718. (b) O'Ferrall, R. A. M. Relationships between E2 and E1cb Mechanisms of B-Elimination. *J. Chem. Soc. B: Phys. Org.* **1970**, 274-277.
- (6) (a) Foster, J. P.; Weinhold, F. Natural Hybrid Orbitals. *J. Am. Chem. Soc.* **1980**, *102*, 7211-7218. (b) Reed, A. E.; Weinstock, R. B.; Weinhold, F. Natural Population Analysis. *J. Chem. Phys.* **1985**, *83*, 735-746.
- (7) (a) Liu, F.; Paton, R. S.; Kim, S.; Liang, Y.; Houk, K. N. Diels-Alder Reactivities of Strained and Unstrained Cycloalkenes with Normal and Inverse-Electron-Demand Dienes: Activation Barriers and Distortion/Interaction Analysis. *J. Am. Chem. Soc.* **2013**, *135*, 15642-15649. (b) Chen, S. M.; Huang, X. Q.; Meggers, E.; Houk, K. N. Origins of Enantioselectivity in Asymmetric Radical Additions to Octahedral Chiral- α -Rhodium Enolates: A Computational Study. *J. Am. Chem. Soc.* **2017**, *139*, 17902-17907.